Marine Geology 259 (2009) 86–101

Contents lists available at ScienceDirect

Marine Geology

journal homepage: www.elsevier.com/locate/margeo

Onshore sediment transport on a sandy beach under varied wave conditions: Flow velocity skewness, wave asymmetry or bed ventilation?

Martin Austin [a,*], Gerhard Masselink [b], Tim O'Hare [a], Paul Russell [a]

[a] School of Earth, Ocean and Environmental Sciences, University of Plymouth, Drake Circus, Plymouth, Devon, PL4 8AA UK
[b] School of Geography, University of Plymouth, Drake Circus, Plymouth, Devon, PL4 8AA UK

ARTICLE INFO

Article history:
Received 19 June 2008
Received in revised form 8 January 2009
Accepted 12 January 2009

Keywords:
suspended sediment
cross-shore transport
flow velocity acceleration
bed ventilation
flow velocity skewness
flow velocity asymmetry
macrotidal beach

ABSTRACT

Measurements of the cross-shore suspended sediment flux obtained from a planar and barred beachface have been used to investigate the propensity for wave-driven onshore sediment transport during medium energy conditions. Three processes capable of transporting sediments onshore–flow velocity skewness, wave asymmetry and bed-ventilation were investigated to determine their relative importance. Onshore-directed flow accelerations under the steep front face of asymmetric waves were significantly correlated with sediment suspension, whilst the effects of flow skewness and bed-ventilation were discounted. An acceleration-modified form of the Meyer-Peter-type formula is used as initial attempt at modelling the onshore transport using a temporal filter to modify the bed shear stresses.

1. Introduction

Measurements of cross-shore sediment transport on sandy beaches have shown that the direction of net transport is determined by the relative importance of the mean and oscillatory components of the incident wave motions (Osborne and Greenwood, 1992; Thornton et al., 1996; Aagaard et al., 2002). Energetics-based transport models relate sediment transport to the velocity field close to the bed (after Bagnold, 1966), where wave stirring acts to mobilise the bed sediments (Huntley and Hanes, 1987), which are subsequently transported by the mean currents. When mean currents have been strong (typically under energetic conditions), models based on this assumption (e.g. Thornton et al., 1996; Gallagher et al., 1998) have been able to predict observed morphological change with a reasonable degree of accuracy. However, under calm conditions, when oscillatory wave-motions dominate, these same models perform poorly and generally cannot predict onshore sediment movement because they remain dominated by the offshore-directed mean flow (Schoonees and Theron, 1995; Gallagher et al., 1998; Hsu et al., 2006). The few examples of when energetics models have been able to successfully predict onshore transport have been when three-dimensional circulation has existed (e.g. Aagaard et al., 1998, 2006), whereby the mass flux of the waves is returned seawards through long-shore feeder and rip channels rather than through the bed return flow (e.g. Masselink et al., 2008a). The limited ability of the energetics-type models to predict the onshore drift of sediments during moderate energy conditions suggests that flow velocity skewness is insufficient to drive the observed onshore sediment transport. This has led to the suggestion of (at least) two additional processes, which are correlated with sediment entrainment, flow acceleration (Hanes and Huntley, 1986) and bed ventilation (Conley and Inman, 1994), both of which may promote onshore sediment transport.

As incident waves shoal they become positively skewed with a peaked, narrow crest and flat, wide trough; the strongest flow velocities are therefore directed onshore. Maximum values of flow velocity skewness have been reported from the wave breaker zone (Doering and Bowen, 1987) and this has subsequently been linked to sediment transport. Roelvink and Stive (1989) found that flow skewness provided a significant contribution to the transport, while Thornton et al. (1996), Russell and Huntley (1999) and Marino-Tapia et al. (2007) demonstrate in the field that the dominant transport mechanism outside the surf zone is onshore transport due to flow velocity skewness.

Waves become increasingly asymmetric throughout wave transformation, in particular just prior to and during wave breaking, with pitched forward, steep leading faces and more gently sloping rear faces (Elgar et al., 2001). This results in strong fluid velocity accelerations under the steep leading face of the asymmetric wave

* Corresponding author.
E-mail addresses: martin.austin@plymouth.ac.uk (M. Austin), g.masselink@plymouth.ac.uk (G. Masselink), tohare@plymouth.ac.uk (T. O'Hare), prussell@plymouth.ac.uk (P. Russell).

0025-3227/$ – see front matter © 2009 Elsevier B.V. All rights reserved.
doi:10.1016/j.margeo.2009.01.001

(Elgar et al., 1988). Based on laboratory data, King (1991) noted that asymmetric waves transported significantly more sediment than sine waves, whilst in the field, Hanes and Huntley (1986) showed that the strong flow velocity accelerations that occur under the steep wave faces are correlated with sediment entrainment from the seabed. Field measurements have also shown that maximum acceleration is closely correlated with the location of nearshore sandbar crests (Elgar et al., 2001) and an energetics model extended to include acceleration (Hoefel and Elgar, 2003) suggests that onshore bar migration is related to cross-shore gradients in flow acceleration. Conley and Beach (2003) have also shown that acceleration is significantly correlated with the incident wave frequency suspended sediment flux on a dissipative multi-barred beach.

Bed ventilation, or the cyclic infiltration/exfiltration of water through a saturated bed under waves, can modify patterns of sediment transport (Longuet-Higgins and Parkin, 1962). Two contrasting (and opposing) mechanisms exist: (1) seepage forces change the effective particle weight of the surficial sediments (Martin and Aral, 1971); and (2) the boundary layer structure and shear stresses at the bed are altered (Conley and Inman, 1994). Infiltration exerts a downward-acting seepage force on the bed, but coincidently draws the streamlines closer to the bed, 'thinning' the boundary layer and increasing the bed shear stress; exfiltration results in the opposite. These processes have been investigated in the swash zone with contrasting results. Turner and Masselink (1998) show that the effects of bed ventilation are most significant during uprush, where the effect of altered bed stresses dominate with a 40% increase in the observed transport rate. However, Butt et al. (2001) found the opposite, with the reduction in effective particle weight causing an increase in backwash sediment transport by about 4.5%; a grain size dependence was suggested to shift the dominance from boundary layer effects to stabilisation–destabilisation with decreasing grain size (Nielsen, 1998; Butt et al., 2001; Karambas, 2003).

At this point it is worth clearly re-defining the terms skewness and asymmetry and how they relate to fluid velocity and acceleration. While skewness defines the third moment of a quantifiable parameter such as fluid velocity, it is used to describe the evolution of a shoaling surface gravity wave as the wave crests become sharply peaked and the troughs broad and flat (Bowen, 1980). The fluid velocity skewness (third moment of the velocity) is used to parameterise this wave-shape evolution (Bailard, 1981). Asymmetry describes the evolution of the wave shape just prior to breaking and in the surf zone where waves become pitched forwards with steep front faces and more gently sloping rear faces. This results in asymmetrical wave orbital velocities and therefore skewed fluid accelerations, with larger accelerations under the steep onshore face of the wave (leading the maximum onshore-directed velocity) than under the gently sloping rear face. Therefore, fluid acceleration (flow velocity acceleration) becomes a useful means of quantifying the asymmetric nature of waves, encapsulating a number of processes such as the phase shift of the bed shear stress and the time-varying pressure gradient force. Throughout this paper we are therefore using fluid acceleration as a proxy for onshore wave asymmetry.

Flow velocity skewness, fluid accelerations and bed ventilation all have the potential to cause onshore sediment transport under moderate wave conditions across the nearshore. The purpose of this paper is to test the three processes above and to determine whether one process dominates in the nearshore environment, or alternatively, whether the three processes are collectively responsible for the observed onshore transport. We use field data from two contrasting beaches, one planar and the other barred, collected over periods when both experienced prolonged periods of accretion under medium wave conditions and erosion under high-wave conditions. The first part of the paper describes the experimental methods including a description of the field sites, the measurements collected and the steps involved in processing the data. The second section reports detailed analyses of the hydro- and sediment dynamic process occurring in the intertidal zone. It provides a description of the magnitude and phasing of the flow velocity asymmetry, skewness and bed ventilation in relation to sediment entrainment. The third section utilises these findings in an initial attempt to predict the cross-shore sediment flux over a range of time scales using a modified Meyer-Peter and Müller (1948) approach and demonstrates the importance of flow velocity asymmetry. The final two sections discuss and summarise the results.

2. Methods

2.1. Field sites

A 3-week field campaign was conducted on Sennen Beach, Cornwall, England in May 2005. Sennen Beach is a 2-km long embayed beach and the measurements reported here were conducted in the centre of the embayment (Fig. 1). The beach experiences a mean spring range of 5.3 m and has an average significant wave height of approximately 1.4 m (Davidson et al., 1998). The beach can be classified as a low-tide terrace beach (Masselink and Short, 1993), and is characterized by a steep upper part ($\tan\beta = 0.08$) and a gently-sloping lower section ($\tan\beta = 0.03$). The transition between these two profile segments is located around the mean high water neap (MHWN) level and the steep part of the beach profile is therefore mainly affected by high-tide swash processes. The size and settling velocity distribution of the bed material at the instrument location, determined for a single sample collected during low tide 19, using sieving and a settling tube, indicate a predominance of coarse sediments: the median sediment size and settling velocity were $D_{50} = 0.7$ mm and $w_s = 8$ cm s^{-1}, respectively. These values are representative for the whole beach (Masselink et al., 2007a).

A similar field experiment was conducted over a spring-to-spring tidal cycle in May 2006 on Truc Vert beach, France. Truc Vert experiences a mean spring tide range of 4.3 m and is subjected to a prevailing westerly swell with an average significant wave height of 1.3 m and typical significant wave heights during storms of 5 m (De Melo Apoluceno et al., 2002). A subtidal crescentic bar system is located c. 500 m offshore and the lower intertidal beach is characterised by an intertidal bar system (Sénéchal et al., 2002). The subtidal bar system protects the intertidal beach from exposure to extreme wave conditions; therefore, inshore significant wave heights are generally less than 2.5 m, even during spring high tide, when the protection offered by the crescentic bar is least. The upper intertidal beach is significantly steeper than the lower intertidal beach and a pronounced berm is usually present, especially during the summer months. The median sediment size and settling velocity on the beach were $D_{50} = 0.40$ mm and $w_s = 5.4$ cm s^{-1}, respectively and the upper intertidal beach was coarser than the lower intertidal (Masselink et al., 2008b).

2.2. Beach morphology

A main survey line was established on each beach, extending from the top of the foredune to approximately the mean low water level; two additional transects were set out 20 m either side of the central transect. Temporary benchmarks were installed at the landward ends of the transects and their elevations reduced to ODN and NM (Ordnance Datum Newlyn and Niveau Moyen at Sennen and Truc Vert, respectively) using a real time kinematic global positioning system. Every low tide, the three transects were surveyed using a laser total station to an accuracy O (mm).

2.3. Hydro- and sediment dynamics

During the field surveys, multiple instruments rigs were deployed in a cross shore transect across the intertidal beachface. The main rig

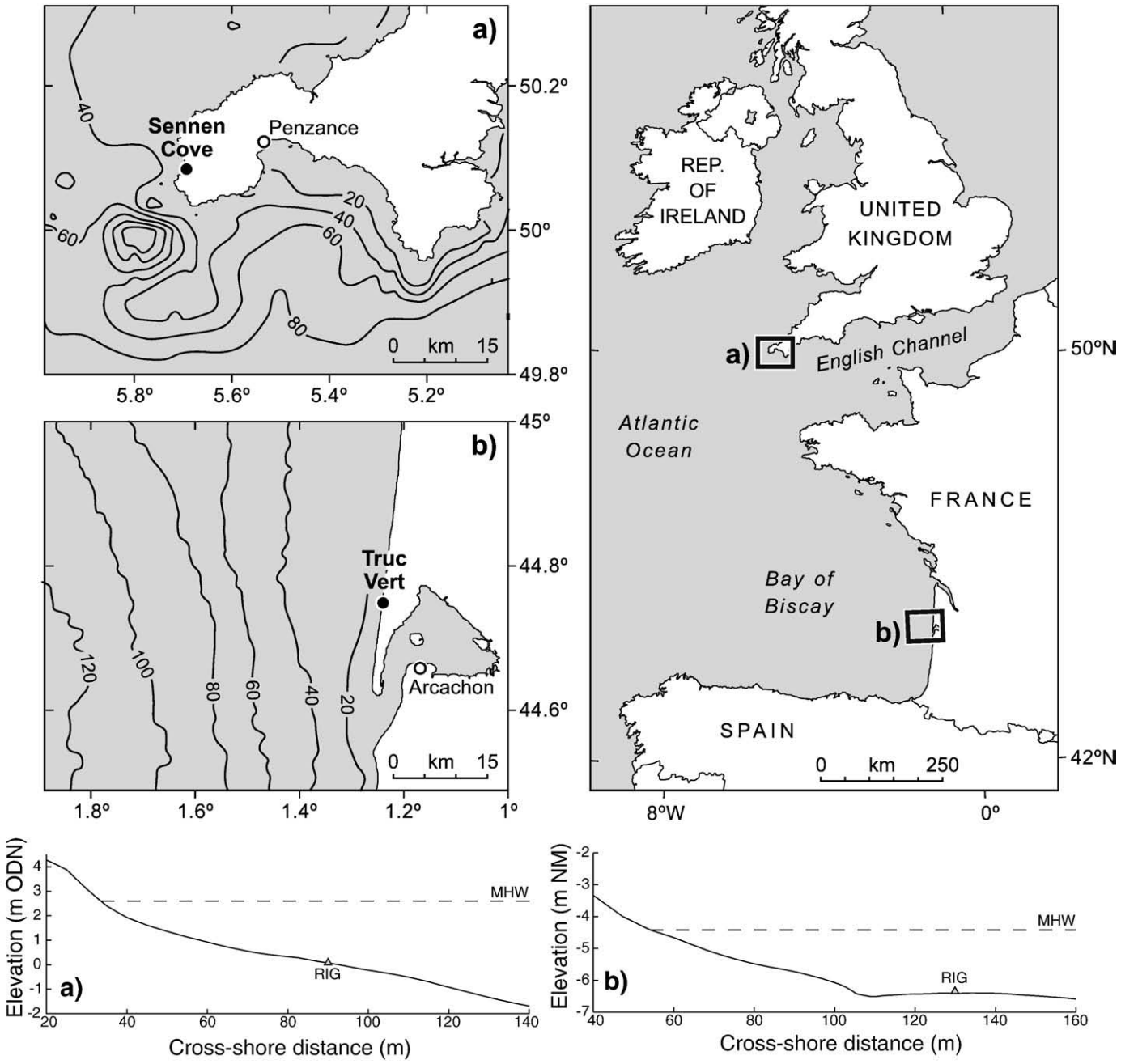

Fig. 1. Location and beach profiles of (a) Sennen Cove and (b) Truc Vert. The cross-shore position of the main instrument rigs are located on the profiles and the dashed lines indicate the mean high water levels.

was located around mid-tide level, which approximately corresponds to mean sea level (MSL), such that over a tidal cycle it was exposed to periods of both breaking and shoaling waves. Flow velocity was measured using six miniature bi-directional Valeport electromagnetic current meters (ECM) deployed to record flow velocities normal and perpendicular to the shoreline at 3, 6, 9, 13, 19 and 29 cm from the bed. The water depth was measured using a pair of pressure transducers (PT) installed 2 and 12 cm below the sand surface. Atmospheric pressure, recorded when the PT was emerged at low tide, was subtracted from the calibrated data and the water depth was determined by assuming that a pressure of 0.01 Pa is equivalent to a 1 cm head of water. A vertical array of miniature optical backscatter sensors (OBS) were used to measure the suspended sediment concentration at −2, −1, 0, 1, 2, 3, 4, 5, 6, 9, 13 and 19 cm from the bed. These were calibrated by suspending known quantities of local sediment in glycerol using the method developed by Butt et al. (2002); the sensor faces were aligned parallel to the wave-induced flow following Ludwig and Hanes (1990).

The OBS data were adversely affected by sunlight and only data collected during night time was used. The OBS sensors could also be used to record bed level changes, because when individual sensors became buried by accretion, their output was maximum. The bedform morphology was monitored across a 2-m long cross-shore profile using two acoustic Sand Ripple Profilers (SRP) mounted 0.7 m above the bed, which collected one acoustic swath every minute. A single-point altimeter was deployed 0.4 m above the bed to provide additional information on the bed level. All main rig instruments were cabled to shore-based computers where the data were synchronously logged at 4 Hz. Offshore wave conditions at Sennen were measured throughout the field survey with an acoustic Doppler

current profiler (ADCP) moored 1 km offshore in ~14 m water depth. At Truc Vert, offshore wave height was obtained from a WaveWatch III model output computed for a grid cell 300 km seaward of the beach (Ardhuin et al., 2007).

To quantify the hydrodynamic conditions a number of non-dimensional parameters were computed from the data. These include the related normalised flow velocity skewness

$$\langle u^3\rangle_n = \langle u^3\rangle / \langle u^2\rangle^{1.5} \tag{1}$$

where u is the cross-shore velocity (defined as normal to the shoreline and positive in the onshore direction), normalised flow acceleration skewness

$$\langle a^3\rangle_n = \langle a^3\rangle / \langle a^2\rangle^{1.5} \tag{2}$$

where a is the cross-shore flow velocity acceleration and normalised ventilation skewness

$$\langle w^3\rangle_n = \langle w^3\rangle / \langle w^2\rangle^{1.5} \tag{3}$$

where w is the vertical seepage velocity, defined as flow perpendicular to and through the seabed surface (positive out of the bed).

2.4. Sediment transport modelling

Our approach is to relate the suspended sediment transport to the flow conditions using a Meyer-Peter and Müller type of formula that relates the dimensionless transport rate Φ to the Shields parameter θ according to

$$\Phi = m\theta^n \tag{4}$$

where m and n are constants with typical values of 12 and 1.5, respectively, for large bed shear stresses (Nielsen, 1992) and

$$Q = \Phi\sqrt{(s-1)gD_{50}^3} \tag{5}$$

where Q is the volumetric sediment transport rate (in $m^3 s^{-1}$ per unit width beachface), s is the ratio between sediment density and water density ρ_s/ρ (2.65), g is acceleration due to gravity (9.8 m s^{-2}) and D_{50} is the median sediment size (0.0007 m at Sennen, 0.0004 m at Truc Vert).

Although initially developed for bedload and sheet flow conditions, when calibrated with the suspended load, models of this type frequently provide better results than models designed for suspended load (e.g. Butt et al., 2004). This ambiguity may be partially explained by considering the mode of transport. For a grain diameter of 0.3 mm (similar to Truc Vert), Bagnold (1966) predicts that bedload will predominate for $\theta<0.18$, whereas suspended load will be fully developed at $\theta>0.35$ and sheet flow at $\theta>0.8$ (Wilson, 1988). Nonetheless, the theoretical arguments of Nielsen (1992) imply that bedload is the principal transport mode during sheet flow conditions, notwithstanding the fact that the threshold for fully developed suspended load has been exceeded and significant suspended load must therefore be present.

The Shields parameter θ is conventionally defined as

$$\theta(t) = \frac{\tau(t)}{\rho(s-1)gD_{50}} \tag{6}$$

where τ is the bed shear stress (in N m^{-2}). For wave motion, τ can be described by

$$\tau(t) = 0.5\rho f_w u(t)|u(t)| \tag{7}$$

were f_w is the wave friction factor and u is the free-stream cross-shore current velocity (in m s^{-1}). The wave friction factor f_w is generally approximated following Swart (1974) as

$$f_w = \exp\left[5.5\left(\frac{2.5D_{50}}{A}\right)^{0.2} - 6.3\right] \tag{8}$$

where A is the wave orbital semi-excursion (in m), which for irregular waves with a peak wave period of T_p (in s) can be computed as

$$A = \frac{\sqrt{2}T_p}{2\pi}\sigma_u \tag{9}$$

and σ_u (in m s^{-1}) is the standard deviation of the cross-shore current velocity.

The Shields parameter θ can be modified to account for the effects of through-bed flow using the approach of Turner and Masselink (1998), who considered the two principal effects of in/exfiltration on sediment mobility: changing weight of surficial sediments due to suction/blowing and altered bed shear stresses due to boundary layer thinning/thickening. These two effects occur independently and can be combined to obtain a modified Shields parameter θ_{gw} given by

$$\theta_{gw}(t) = \theta(t)\left[\frac{1}{1-\frac{1}{2(s-1)}\frac{w(t)}{K}}\right]\left[\frac{c\frac{w(t)}{u(t)}/f_w}{\exp\left(c\frac{w(t)}{u(t)}/f_w\right)-1}\right] \tag{10}$$

were w is through-bed velocity (in m s^{-1}), K is hydraulic conductivity (in m s^{-1}) and c is a constant ($c=0.9$ for oscillatory flow; Conley and Inman, 1994). It is noted that Eq. (10) differs from Eq. (28) in Turner and Masselink (1998) due to a mistake in the latter. The through-bed velocity is obtained using Darcy's law for 1D vertical flow in porous media given by

$$w = -K\frac{dh}{dz} \tag{11}$$

where dh/dz is the vertical hydraulic gradient. The hydraulic conductivity K is a notoriously difficult parameter to quantify and was estimated to be 0.001 m s^{-1}, based on the sediment characteristics (size and sorting) and the equation of Krumbein and Monk (1942). In Eq. (10), the first term in brackets represents the changing weight of surficial sediments and the second term represents altered bed shear stresses.

The processes encapsulated by flow acceleration/deceleration have been modelled using the time-domain filter method of Nielsen and Callaghan (2003), based on the method developed by (Nielsen, 1992, pp. 121–128). This approach first generates a 'sediment mobilising velocity' u_θ given by

$$u_\theta(t) = \sqrt{0.5f_w}\left(\cos\varphi_\tau u(t) + \sin\varphi_\tau\frac{1}{\omega_p}\frac{du}{dt}\right) \tag{12}$$

were ω_p is the peak wave frequency and the angle φ_τ controls the weightings of the drag forces and pressure gradients (acceleration). For $\varphi_\tau=0°$ the drag forces dominate, whereas for $\varphi_\tau=90°$ the pressure gradient (acceleration) is dominant. Nielsen (2006) calibrated Eq. (12) using laboratory data and found an optimal angle of $\varphi_\tau=51°$. The sediment mobilising velocity u_θ is incorporated into a Shields parameter θ_{acc} according to

$$\theta_{acc}(t) = \frac{u_\theta(t)|u_\theta(t)|}{(s-1)gD_{50}}. \tag{13}$$

The instantaneous sediment flux was then predicted with a Meyer-Peter and Müller (1948) type equation using the standard Shields parameter and a critical Shields parameter of $\theta_c = 0.05$

$$Q_p(t) = \begin{cases} 12[|\theta(t)| - \theta_c]^{1.5} \dfrac{u(t)}{|u(t)|}\sqrt{(s-1)gD_{50}^3} & \text{for } |\theta(t)| \geq \theta_c \\ 0 & \text{for } |\theta(t)| < \theta_c \end{cases} \quad (14)$$

and Shields parameters modified for in/exfiltration

$$Q_p(t) = \begin{cases} 12\left[|\theta_{gw}(t)| - \theta_c\right]^{1.5} \dfrac{u(t)}{|u(t)|}\sqrt{(s-1)gD_{50}^3} & \text{for } |\theta(t)| \geq \theta_c \\ 0 & \text{for } |\theta(t)| < \theta_c \end{cases} \quad (15)$$

and acc/deceleration

$$Q_p(t) = \begin{cases} 12[|\theta_{acc}(t)| - \theta_c]^{1.5} \dfrac{u(t)}{|u(t)|}\sqrt{(s-1)gD_{50}^3} & \text{for } |\theta(t)| \geq \theta_c \\ 0 & \text{for } |\theta(t)| < \theta_c \end{cases} \quad (16)$$

3. Results

During the Sennen field campaign, data were collected during 37 consecutive tidal cycles over a range of wave conditions ($H_s = 0.3$–1.6 m; $T_p = 5$–11 s) and water depths (<1–2.5 m) (Fig. 2). The morphological change was characterised by steady accretion until high tide (HT) 29, which resulted in an initial steepening of the upper-beachface followed by the formation of a small intertidal bar at $x = 75$ m by HT28. Subsequently, the beach rapidly erodes, returning to a concave profile by HT38. Over the entire field campaign, the upper beach volume decreased by 2 m^3m^{-1}.

At Truc Vert, data were collected over 24 consecutive high tides characterised by two distinct phases of wave forcing (Fig. 3). Phase one (HT03-H22) was dominated by moderate inshore wave conditions ($H_s = 0.3$–0.75 m; $T_p = 10$ s) during which progressive accretion characterised by berm construction occurred. After HT23, high inshore wave conditions prevailed with $H_s = 0.75$–1.4 m and $T_s = 12$–15 s, which caused the rapid infilling of the landwards trough of the intertidal bar and the formation of a concave profile (see Masselink et al., 2008b). Over the entire field campaign, in the region between the main rig and the shoreline, Truc Vert experienced c. 8 m^3m^{-1} of accretion.

The suspended sediment data suffered from two saturation issues. During day-light hours, the OBS sensors were saturated by ambient light (cf. Masselink et al., 2007b) and, under the energetic wave conditions experienced at the end of the Truc Vert experiment, by wave breaking-induced aeration. Due to the phasing of the tides, more complete tidal cycles occurred during the hours of darkness at Sennen than Truc Vert; therefore, the suspended sediment data collected during the Sennen field campaign were used for the subsequent analysis. The offshore wave climate experienced over the 22 days spanning the middle of the field campaign were very consistent and

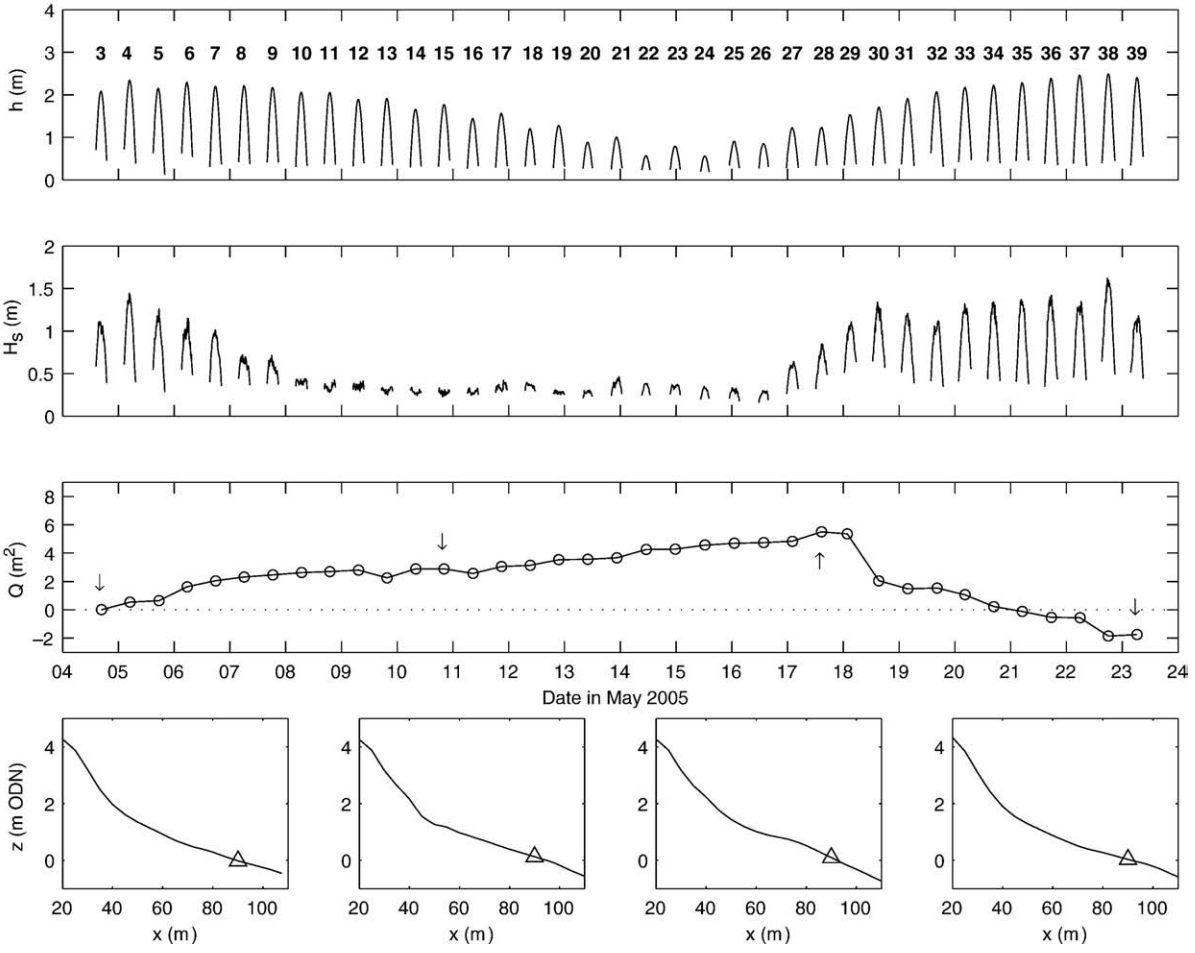

Fig. 2. Event summary of conditions at Sennen. From top–water depth h; significant wave height H_s; variation in the intertidal beach volume landwards of the main rig; and selected beach profiles at the times indicated by the arrows in the beach volume plot. The sediment volume was computed relative to the volume at LT03 and the results were averaged over the three transects. The triangles indicate the location of the instrument rig.

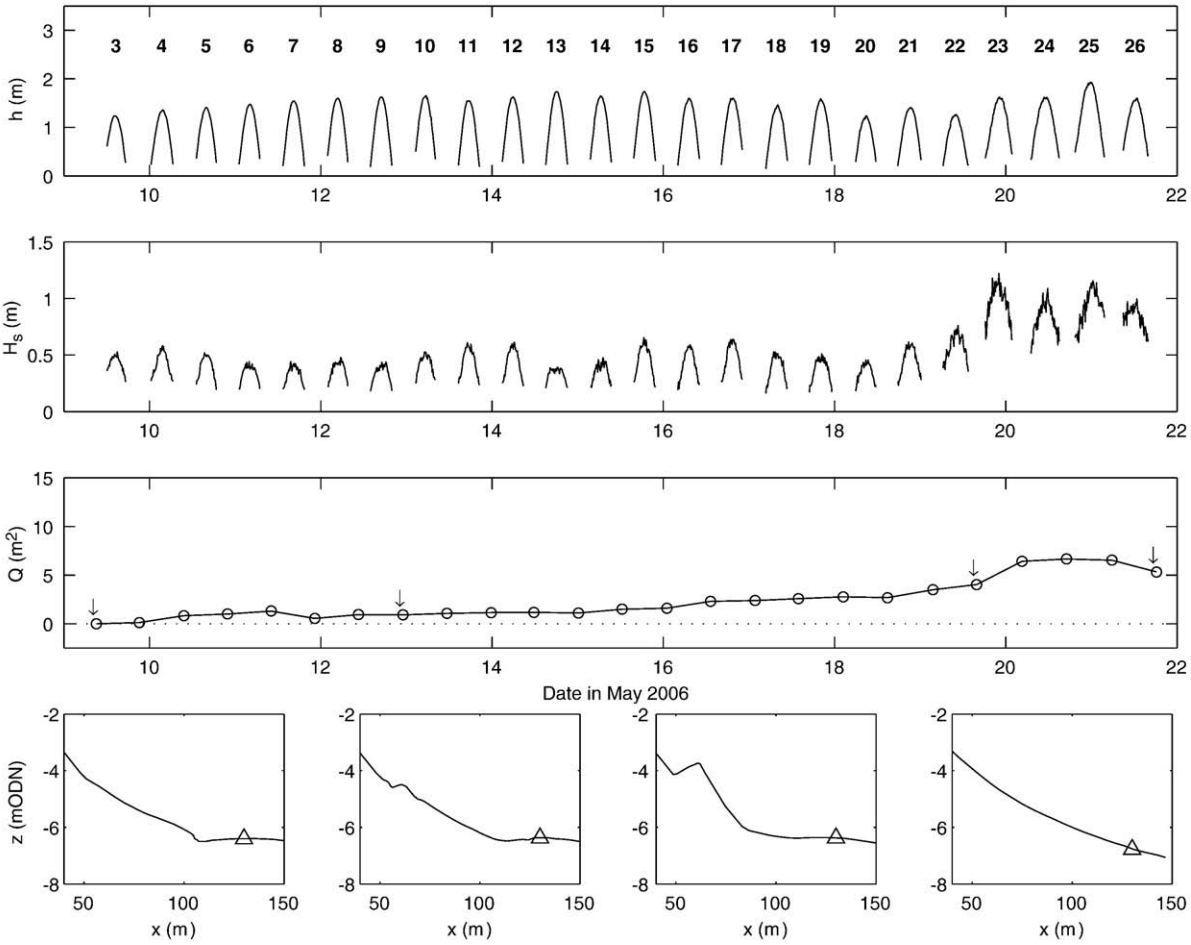

Fig. 3. Event summary of conditions at Truc Vert. From top–water depth h; significant wave height H_s; variation in the intertidal beach volume landwards of the main rig; and selected beach profiles at the times indicated by the arrows in the beach volume plot. The sediment volume was computed relative to the volume at LT03 and the results were averaged over the three transects. The triangles indicate the location of the instrument rig.

any tide can be considered representative of the conditions experienced. In the following, the conditions measured at Sennen during HT27 (18–19 May 2005) are considered. Later in the paper, the Truc Vert data are discussed.

3.1. Bed-level correction

A necessary step in the data analysis is correcting the suspended sediment and flow velocity time series for bed-level changes due to migrating wave ripples; typical ripple height and length during the experiment were 6–9 and 30–40 cm, respectively (Masselink et al., 2007b). A record of the bed level was derived from the vertical stack of OBS sensors by identifying those sensors that were buried. Then using the method outlined by Austin and Masselink (2008), the suspended sediment concentrations and flow velocities at cm-intervals above the bed level from $z = 1$–15 cm were determined through linear interpolation of the vertical stacks of sensors. The result of this adjustment are time series of u and c, at 1 cm intervals, in a layer with a constant elevation of 1–15 cm above the bed, regardless of the ripples migrating under the instruments. The product of the individual u and c time series then provides the depth-integrated suspended sediment flux q when averaged over the lowest 15 cm.

3.2. Hydro- and sediment dynamics

Fig. 4 shows a 1-min example time series of hydro- and sediment-dynamic data collected just before 03:00 h during HT27, when the instrument rig was located in the surf zone and subjected to a mixture of breaking and broken waves. The shape of the waves is clearly asymmetric, characterized by steep fronts and gently-sloping backs, and all plotted parameters exhibit a pronounced asymmetry over individual wave cycles. Onshore flows are stronger than offshore flows, and sediment is mainly suspended under wave crests. Significant amounts of sediment are suspended up to 0.1 m from the bed and most suspended sediment settles back to the bed before commencement of the offshore stroke of the wave. The concurrence of high suspended sediment concentrations with the onshore stroke of the wave results in a dominant net onshore suspended sediment flux. Infiltration (negative w/K) and flow acceleration (positive a) occur under wave crests, whereas exfiltration and deceleration occur under wave troughs.

Hydro- and sediment-dynamic parameters were computed for 10-min data segments collected during HT27 (Fig. 5). At high tide, the instrument rig was located close to the break point with a mean water depth of $\langle h \rangle = 1.3$ m and significant wave height of $H_s = 0.6$ m. The mean cross-shore flow velocity $\langle u \rangle$ was consistently offshore with typical speeds of 0.1–0.2 m s^{-1} during the rising a falling tide (inner- and mid-surf zone), and near-zero flows around high tide (outer surf zone). The maximum wave orbital velocity U_m was 1.5 m s^{-1} a occurred around high tide. The normalised flow velocity skewness $\langle u^3 \rangle_n$ was negative during the rising and falling tide, but near-zero around high tide. The time series of the mean suspended sediment concentration $\langle c \rangle$ over the lower 0.15 m of the water column shows the same pattern of variation as U_m and $\langle u^3 \rangle_n$, with a maximum of 5–10 kg m^{-3} around high tide and lower values ding the rising and falling tide. The suspended sediment flux $\langle q \rangle$ was dominated by the onshore-directed oscillatory flux, with

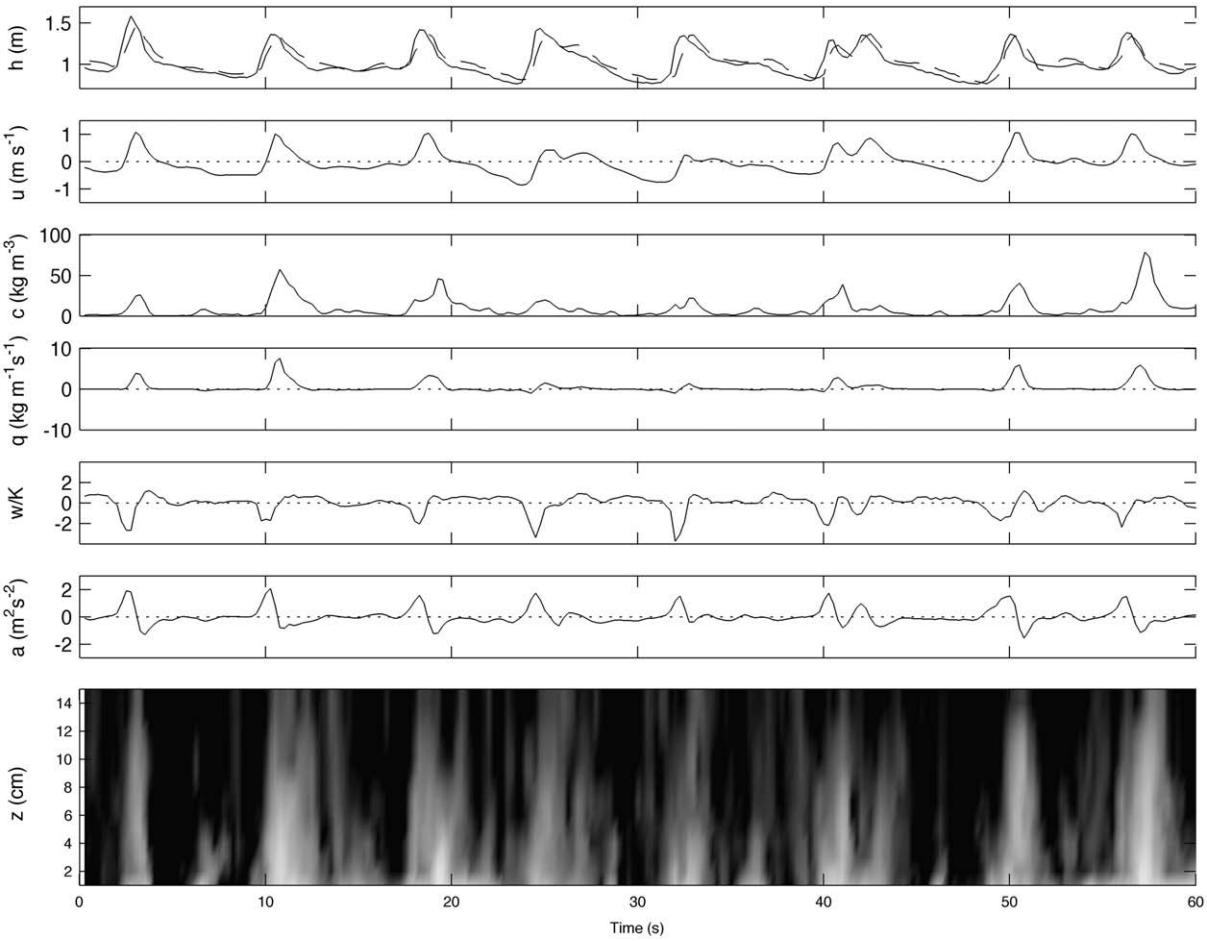

Fig. 4. Example time series collected just before 03:00 h during HT27 showing: water depth h; cross-shore current velocity u measured at 0.13 m above the bed; suspended sediment concentration c averaged over the lower 0.15 m of the water column; depth-averaged suspended sediment flux q over the lower 0.15 m of the water column; vertical pressure gradient in the bed w/K; flow acceleration a; and the vertical distribution of suspended sediment. The solid and dashed lines in the upper panel represent the water depth measured 0.02 and 0.12 m below the bed, respectively. The shading in the bottom panel represents the natural log of the sediment concentration between 0 (black) and 6 (white).

the largest fluxes of the or of 2 kg $m^{-1}s^{-1}$ occurring around high tide. The fluctuation in $\langle q \rangle$ at 01:45 hrs is probably associated with migrating wave ripples. Partitioning the sediment fluxes into mean and oscillatory components revealed that the oscillatory flux was onshore and dominated the offshore mean flux. The normalised ventilation and acceleration skewness, $\langle w^3 \rangle_n$ and $\langle a^3 \rangle_n$, did not vary consistently over the tidal cycle and were around -1.5 and 1.5, respectively. These values indicate a dominance of infiltration over exfiltration, and acceleration over deceleration.

Fig. 6 shows the vertical suspended sediment concentration and flux profile, averaged over a 30-min period from 01:45 to 02:15 hrs when the instruments were located in the outer surf zone. It also shows the (normalised) co-spectrum between the cross-shore velocity at $z = 0.13$ m and the suspended sediment concentration at $z = 2$ cm. The vertical profiles are exponential, which is indicative of a diffusion-type sediment transport process (Nielsen, 1986). The mixing length scale l_s, obtained by fitting an exponential curve to the suspended sediment profile is 6 cm, which is to be expected given a ripple height of 6–9 cm (cf., Nielsen, 1992). More than 90% of the suspended sediment load and flux occurs in the lower 0.05 m of the water column. The co-spectrum reinforces the notion that suspended sediment transport is mainly driven by incident waves and is in the onshore direction. The suspended flux is offshore at infragravity-wave frequencies, but this is subordinate to the onshore sediment flux due to incident-wave flux-coupling.

Using the 30-min data section collected from 01:45 to 02:15 hrs, cross-correlations were computed between time series of u, c, a and w to investigate the phasing between the signals (Fig. 7). A positive correlation ($r = 0.22$) exists between u and c at a lag of zero, suggesting these two time series are in phase. Correlations of similar strength are present between w and c ($r = -0.30$), and a and c ($r = 0.30$), but at a negative lag of 0.75 s. The negative lag indicates that peaks (and/or troughs) in the time series of w and a occur before those in c. The cross-correlations between u and w, and u and a show zero correlation at a lag of zero, and correlation peaks of about 0.6 at positive and negative lags of 0.75 s, respectively. The cross-correlations involving w and a are virtually identical, except for the sign, and this is borne out by the cross-correlation between w and a which shows a very high negative correlation ($r = -0.76$) at a lag of zero. The cross-correlations shown in Fig. 7 suggest that the timing of sediment suspension events concurs with maximum onshore flow velocities, and that infiltration coincides with maximum acceleration, both occurring around the time of flow reversal. The time difference between maximum acceleration/infiltration and cross-shore flow velocity/sediment concentration is only 0.75 s, and this is directly attributable to the steep front faces that characterise the waves under investigation (refer to top panel in Fig. 4).

The complete data set collected during HT27 was subjected to wave-by-wave analysis, whereby individual waves were extracted from the data set using a zero-downcrossing routine applied to the cross-shore velocity time series. A sub-set of waves were selected that satisfied the following criteria: (1) the wave period was between 5 and 10 s; (2) both the peak onshore and offshore flow speeds exceeded 0.75 m s^{-1}; and (3) the flow duration asymmetry, defined as the ratio

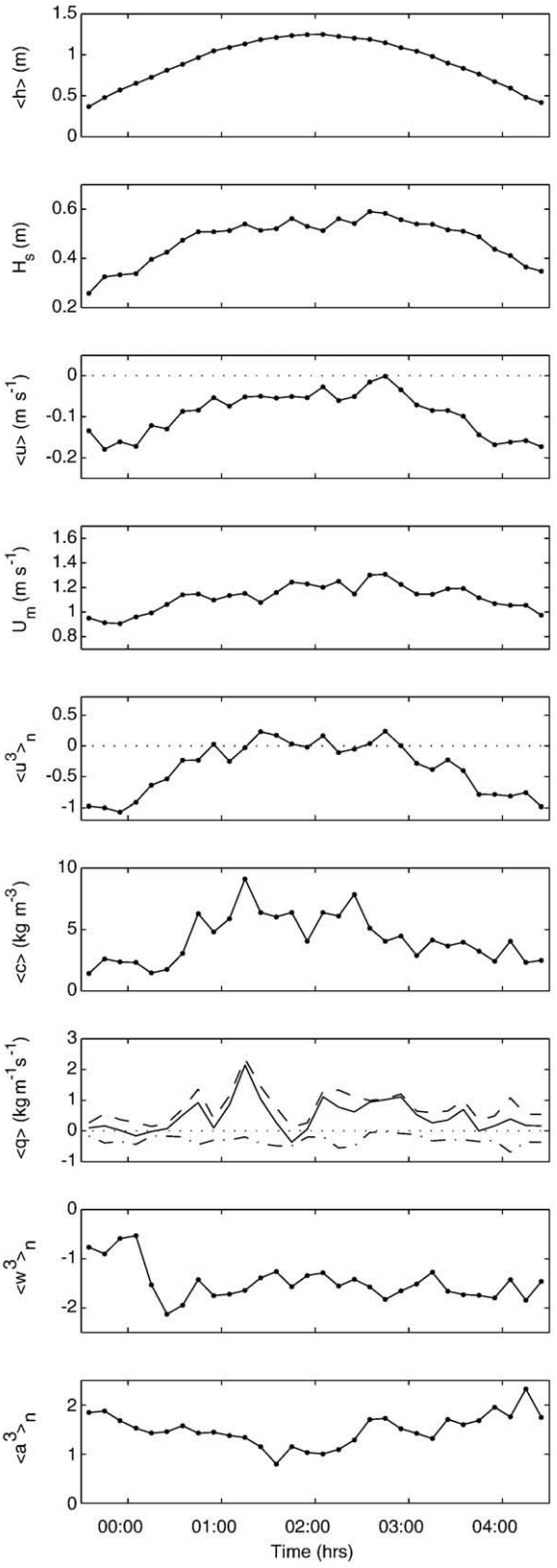

Fig. 5. Temporal variation in time-averaged hydro- and sediment-dynamic parameters computed from 10-min data segments collected during the night high tide of 18–19 May (HT27): water depth $\langle h \rangle$; significant wave height H_s; cross-shore current velocity $\langle u \rangle$ measured at 0.13 m above the bed; maximum wave orbital velocity U_m; normalised velocity skewness $\langle u^3 \rangle_n$; suspended sediment concentration $\langle c \rangle$ averaged over the lower 0.15 m of the water column; net (–), oscillatory (– –) and mean (·–·) suspended sediment flux $\langle q \rangle$ depth-averaged over the lower 0.15 m of the water column; ventilation skewness $\langle w^3 \rangle_n$; and normalised acceleration skewness $\langle a^3 \rangle_n$.

of onshore flow duration to offshore flow duration, is between 0.5 and 2. The latter criterion ensures that the selected waves are relatively 'clean' and do not represent multi-crested wave events. A total of 150 waves satisfied these criteria and the mean suspended sediment concentration $\langle c \rangle$, the rms cross-shore current velocity u_{rms}, the maximum infiltration/exfiltration flow velocity w_m and the maximum flow acceleration/deceleration a_m were computed for the onshore and offshore phases of each of the selected waves. Histograms were then produced showing the frequency distributions of these parameters (Fig. 8). The histograms emphasise the asymmetry in the sediment suspension process, with significantly larger sediment concentrations during the onshore phase of the wave cycle. The distribution of u_{rms} is similar between the on-shore and offshore phases of the wave cycle, suggesting that the suspension asymmetry cannot be attributed to differences in the cross-shore flow velocities. In contrast, the distributions of w_m and a_m are highly asymmetric, with acceleration and infiltration during the onshore phase of the wave cycle far exceeding deceleration and exfiltration during the offshore phase.

The waves plotted in Fig. 8 were characterised by similar u_{rms} distributions for the onshore and offshore phases of the wave cycle, but the peak onshore velocities were generally larger than the peak offshore velocities. The peak onshore and offshore velocity averaged for all the waves was 1.07 m s^{-1} and 0.92 m s^{-1}, respectively. It could thus be argued that the larger suspended sediment concentrations under wave crests are due to the larger peak onshore flow velocities, rather than flow acceleration and/or infiltration. Therefore, a further subset of waves was extracted from the 150 previously selected waves by only considering those waves for which the difference between the peak onshore flow velocity and the peak offshore flow velocity was less than 10%. A total of 42 waves satisfied this later criterion. The time series of h, u, c, w and a for each selected wave was resampled over a (normalised) time axis, running from 0 to 1 (with time steps of 0.01), and the time axis was centred around the zero-upcrossing. The suspended sediment concentration over each wave cycle was normalised by dividing c by the average concentration over the wave cycle $\langle c \rangle$ to avoid biasing the results to the largest events. An ensemble wave was subsequently computed from these normalised waves (Fig. 9). Comparison of the ensemble wave with an example wave indicates that the former is representative.

The shape of the ensemble wave is horizontally-symmetric (peak onshore and offshore velocities are virtually identical), but vertically-asymmetric (steep wave front and gently sloping back). As demonstrated earlier, maximum suspended sediment concentration coincides with the peak onshore flow velocity under the wave crest, and maximum infiltration and acceleration occur at flow reversal. The result clearly demonstrates that the sediment suspension asymmetry over the wave cycle cannot be due to a difference in onshore/offshore flow velocities (flow velocity skewness), and is more likely related to infiltration and/or flow velocity asymmetry.

4. Suspended sediment transport modelling

4.1. Wave-event time scale

The instantaneous suspended sediment flux was predicted using the Meyer-Peter and Müller (1948) type formula, modified according to Eqs. (14)–(16). Fig. 10 shows the same 1-min section of data discussed previously (Fig. 4), together with the modelled instantaneous suspended sediment fluxes computed using the standard and modified Shields parameters. A standard Shields approach grossly underpredicts the onshore suspended sediment transport rate under the wave crests, whilst the offshore transport rate under the wave troughs is predicted quite well. Accounting for through-bed flow makes no significant difference, but accounting for flow acceleration reproduces the observed onshore flux peaks very well.

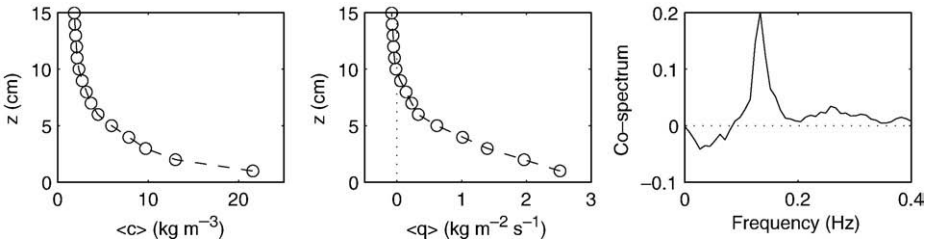

Fig. 6. Vertical profile of suspended sediment concentration and suspended sediment flux, and co-spectrum between (free-stream) cross-shore current velocity and suspended sediment concentration measured at 2 cm above the bed. The data were collected from 01:45 to 02:15 hrs during HT27. The co-spectrum was normalised by dividing the co-spectral estimates by the total co-spectral density integrated over the entire frequency range.

4.2. Tidal cycle time scale

Fig. 11 shows the performance of the sediment transport models over the complete tidal cycle of HT27 for 10-min data segments, and confirms the previous findings: (1) application of a conventional Shields parameter under-estimates onshore suspended sediment transport under wave crests; (2) the effects of through-bed flow are insignificant; and (3) including fluid acceleration correctly predicts onshore suspended sediment transport. The optimal angle φ_τ in the Shields parameter modified for fluid acceleration appears to be between 25 and 50°. The total measured non-dimensional flux over the tidal cycle was 11, whereas the predictions for $\varphi_\tau = 25$ and 50° are 5 and 24, respectively. The drop in the measured onshore suspended flux from 01:30 to 02:00 hrs due to ripple migration is not reproduced.

4.3. Spring-neap time scale

Whilst it is informative to model the suspended sediment flux at time scales of seconds to hours, it is potentially of more use to be able to predict the sediment flux (and hence morphological change) over much longer time scales. The predictions of the suspended sediment flux at wave and tidal cycle time scales highlight the poor ability of the standard Shields model to predict the onshore fluxes under the wave peaks, whilst demonstrating that the effects of through-bed flow are insignificant. The acceleration-modified model (Eq. (16)) is able to replicate the suspended flux with reasonable success and is therefore used to predict the instantaneous sediment transport rate over the entire field campaigns at both Sennen and Truc Vert.

4.3.1. Optimisation of φ_τ based on Sennen field data

The value of the phase angle φ_τ used up to this point was somewhat arbitrary, and based upon the published values obtained from wave flume and u-tube experiments by Nielsen (2006). The Sennen data provide the opportunity to determine an optimal 'field-based' value for φ_τ. A Truc Vert field optimisation was not possible due to the limited availability of suspended sediment data.

Data from three additional tides were analysed following an identical procedure to that set out in Section 3. The measured suspended sediment flux Q_m was computed for each 10-min segment of data and compared to the flux predicted using Eq. (16) (Q_p) using a range of values for φ_τ between 0 ad 90°. The optimal value of φ_τ for each 10-min segment was considered to be that which provided the best correlation between Q_m and Q_p. The average value of φ_τ was taken as the median of the 10-min values recorded over the tidal cycle. The results of the optimisation are shown in Table 1 and the optimal value for φ_τ over the field campaign was $\varphi_\tau = 34.5°$.

4.3.2. Predicted transport at Sennen

The temporal changes in the bed-level due to accretion and erosion over the region of the beachface landwards of the main rig ($x = 90$ m) were computed as a volumetric sediment flux Q from the morphological survey (Fig. 2).

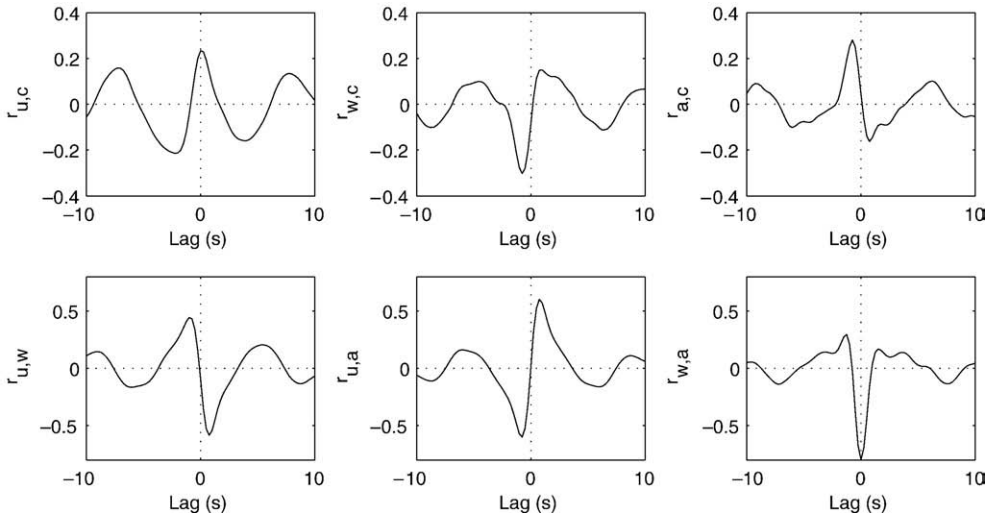

Fig. 7. Cross-correlation r between time series of cross-shore current velocity u measured at 0.13 m above the bed, suspended sediment concentration c averaged over the lower 0.15 m of the water column, vertical flow velocity w and flow acceleration a. The cross-correlations were computed using a 30-min data segment collected during HT27 (01:45–02:15 hrs).

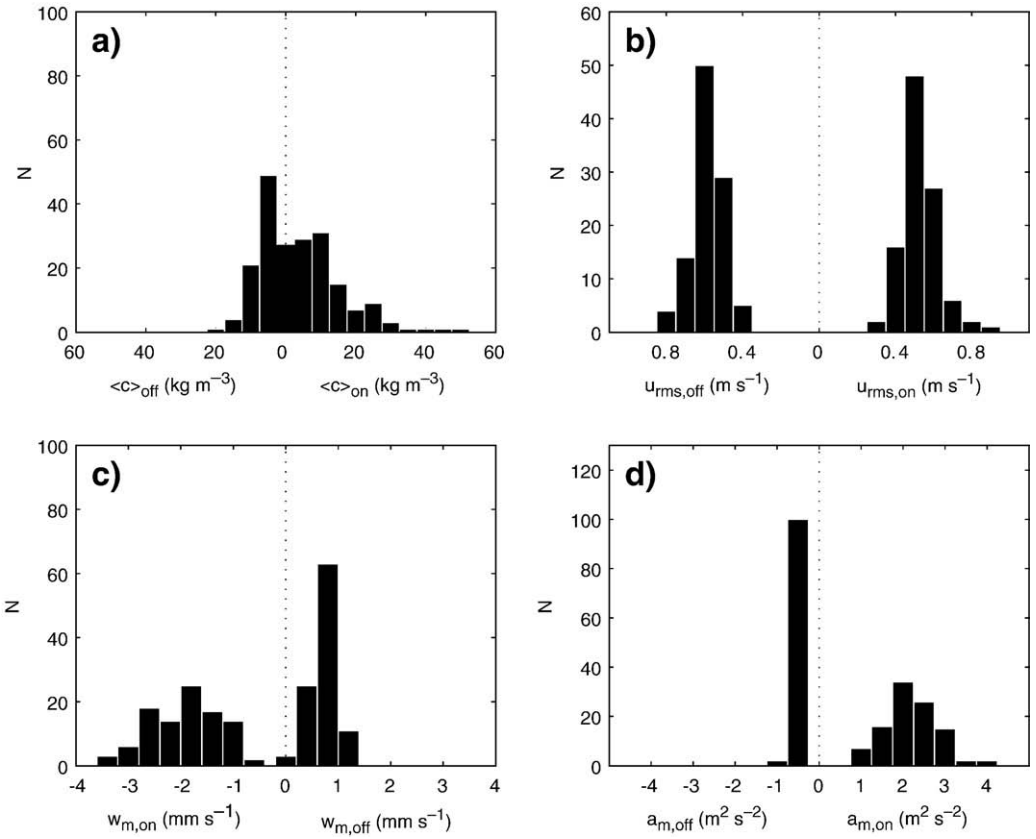

Fig. 8. Absolute frequency distributions of: (a) mean suspended sediment concentration over the lower 0.15 m of the water column averaged over the onshore and offshore phase of the wave cycle $\langle c_{on}\rangle$ and $\langle c_{off}\rangle$; (b) the rms cross-shore current velocity computed over the onshore and offshore phase of the wave cycle $u_{rms,on}$ and $u_{rms,off}$; (c) the maximum infiltration velocity ($w<0$) during the onshore phase of the wave $w_{m,on}$ and the maximum exfiltration velocity ($w>0$) during the offshore phase of the wave $w_{m,off}$; and (d) the maximum flow acceleration ($a>0$) during the onshore phase of the wave $a_{m,on}$, the maximum flow deceleration ($a<0$) during the offshore phase of the wave $a_{m,off}$. The analysis is based on 150 waves extracted from the data collected during HT27.

To make the sediment volumes directly comparable with the measured and predicted suspended fluxes using a mass balance approach, the pore spacing was accounted for as

$$Q = Q(1-n) \tag{17}$$

where n represents the pore space ($n=0.35$).

At Sennen, hydrodynamic data were collected every high tide from 6 May to 26 May (HT03-HT39). Statistical analysis on the time series from the main rig was conducted on 10-min data sections, which was considered the best compromise between the requirement for tidal stationarity and averaging out the natural variability in the conditions. For every data section, the following parameters were computed: mean water depth h, significant wave height H_s significant wave period T_s, mean cross-shore current $\langle u\rangle$, maximum wave orbital velocity U_m, the sediment mobilising velocity u_θ and the acceleration modified Shields parameter θ_{acc}. The predicted vertically-integrated suspended sediment flux Q_p was computed from the later two parameters using values of $\varphi_\tau=0°$ (no acceleration) and $\varphi_\tau=34.5°$ (acceleration). The results are plotted in Fig. 12.

When the fluid accelerations are included, the net sediment transport rate at the beginning of the field campaign under energetic wave conditions is predicted to be offshore. Subsequently, low wave conditions prevail (HT05-H26) and the transport is onshore-directed, but the rates are relatively low at 0.13 m^3. The total predicted transport rate over the calm period is 2.9 m^3. During the energetic conditions experienced at the end of the field campaign (HT27-HT39), the predicted sediment transport rates increase and are frequently offshore-directed; the average predicted transport rate per tidal cycle is 0.37 m^3 (total = 4.9 m^3). Overall, the beach is predicted to gain 7.6 m^3 of sediment. During the strongest offshore events, the largest transport rates occur during the rising and falling tide when the water depths are shallowest, whereas during the strongest onshore events, peak transport occurs during high tide. When fluid accelerations are ignored, the mean cross-shore flow dominates and transport rates are predicted to be strongly offshore-directed with a net loss of -10 m^3 of sediment.

Comparing the predicted and measured sediment fluxes shows that when fluid accelerations are included the general trends in morphological change are reproduced reasonably well, although quantitatively the model predicts a net sediment gain of 7.6 m^3, whereas there was in fact a net loss of -2 m^3. If fluid accelerations are ignored, the model is unable to predict onshore sediment transport and the beach is strongly eroded loosing -10 m^3 of sediment. There are two areas where the acceleration model skill is notably limited: (1) the model predicts strong offshore transport during HT03, which did not occur in the field; and (2) the period of erosion after HT30 is not well reproduced. This suggests that the value of φ_τ requires further optimisation. By reducing the value of φ_τ to 32.5°, the excessive onshore-bias in the predicted transport rate is reduced and there is much better qualitative agreement with the observed morphological change (not shown); however, the incorrectly predicted offshore transport during HT03-HT04 remains.

4.3.3. Truc Vert

The Truc Vert data provides the opportunity to test the general applicability of the acceleration model on a site other than that for which it was optimised. Hydrodynamic data were collected from the main rig every high tide from 9 to 22 May (HT03-HT26). As for Sennen, the sediment flux was predicted with and without fluid accelerations

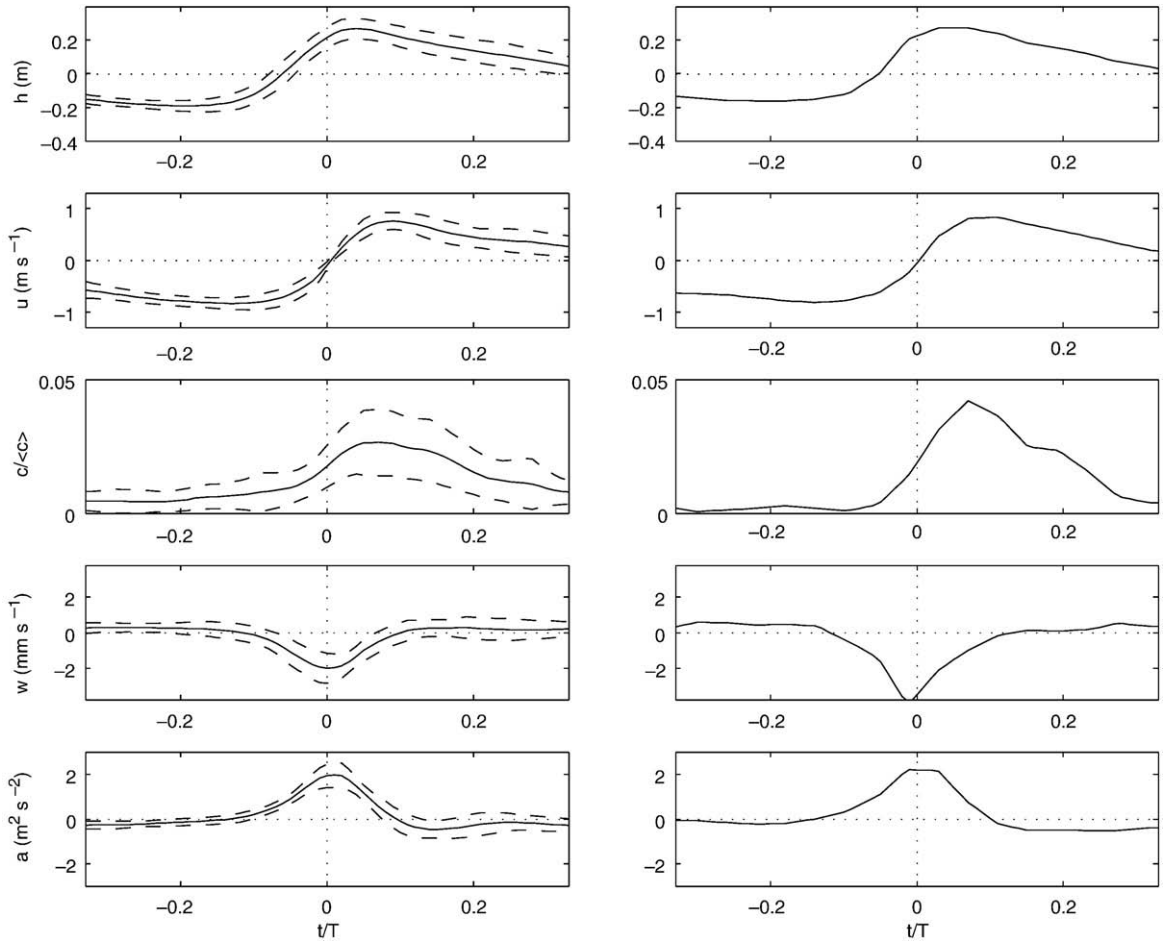

Fig. 9. Ensemble (left) and example (right) wave event, showing: water depth h, cross-shore current velocity u, normalised suspended sediment concentration $c/\langle c\rangle$, vertical flow velocity w and flow acceleration a. The dashed lines for the ensemble wave represent the mean values ± one standard deviation.

using $\varphi_\tau = 34.5°$ (as optimised for Sennen) and $\varphi_\tau = 0°$ (Fig. 13). There is good quantitative agreement with the observed morphological change when acceleration is included, particularly during the moderate conditions during HT7-22; however, whilst the model is qualitatively correct during the energetic HT23-24, it under predicts the flux during these tides. Quantitatively, the net increase in beach sediment landward of $x = 130$m (5.3 m^3; refer to Fig. 3) is a factor of 1.2 of the predicted cumulative transport for the main rig (4.3 m^3). When acceleration is ignored, there is still reasonable qualitative agreement with the measured change until HT22, after which erosion is predicted; quantitatively, the flux is under-predicted by a factor 5 when acceleration is neglected.

5. Discussion

Detailed field measurements of near-bed flow velocities and suspended sediment concentrations from two contrasting sand beaches demonstrate that suspended sediment fluxes under moderate wave conditions were predominantly onshore-directed. This was due to the flux coupling between the oscillatory component of the incident waves and the instantaneous suspended sediment concentration, which dominated over the (offshore-directed) mean flow component. Three processes that might independently cause net onshore transport, flow velocity skewness, wave asymmetry and in/exfiltration have been analysed and the results indicate that the intense positive flow accelerations, which occur during the onshore half-cycle under asymmetric waves, are strongly correlated with the onshore sediment flux. Sediment transport rates computed with a modified Meyer-Peter-type model are shown to reproduce the measured morphological change with a reasonable degree of both qualitative and quantitative accuracy.

The hydrodynamic time series and ensemble wave events clearly demonstrate the asymmetric forward leaning nature of the waves and while cross-correlations show that u and c are in phase, they also reveal that a and w lead suspension events by ~0.75 s; this time lag would appear to be directly attributable to the steep front faces of the waves in question. Additionally, after the steep front of the asymmetric wave initiates the sediment entrainment, the velocity under the gently sloping rear of the asymmetric wave remains directed onshore for a relatively longer time than a wave with velocity skewness alone and the transport remains onshore (Gonzalez-Rodriguez and Madsen, 2007).

The relative importance of fluid accelerations and bed-ventilation were tested by comparing the instantaneous sediment flux predicted using modified forms of the Shields parameter (Eqs. (15) and (16)) to the flux measured over a number of time scales. A standard Shields parameter grossly under-predicts the onshore transport and accounting for in/exfiltration provides no significant improvement. In the swash zone, where maximum infiltration (exfiltration) concurs with maximum onshore (offshore) flow velocities, the importance of in/exfiltration is only of the order 10%, whereas the present field observations suggest that onshore wave-induced flows are several factors more efficient in transporting sediment than the offshore flows ($O(100\%)$). In this context, it is perhaps unsurprising that the inclusion of seepage effects provides a negligible enhancement to predicted sediment fluxes. However, accounting for fluid acceleration reproduces the observed magnitude of the transport peaks very well, although their phasing slightly leads the measured transport, which is

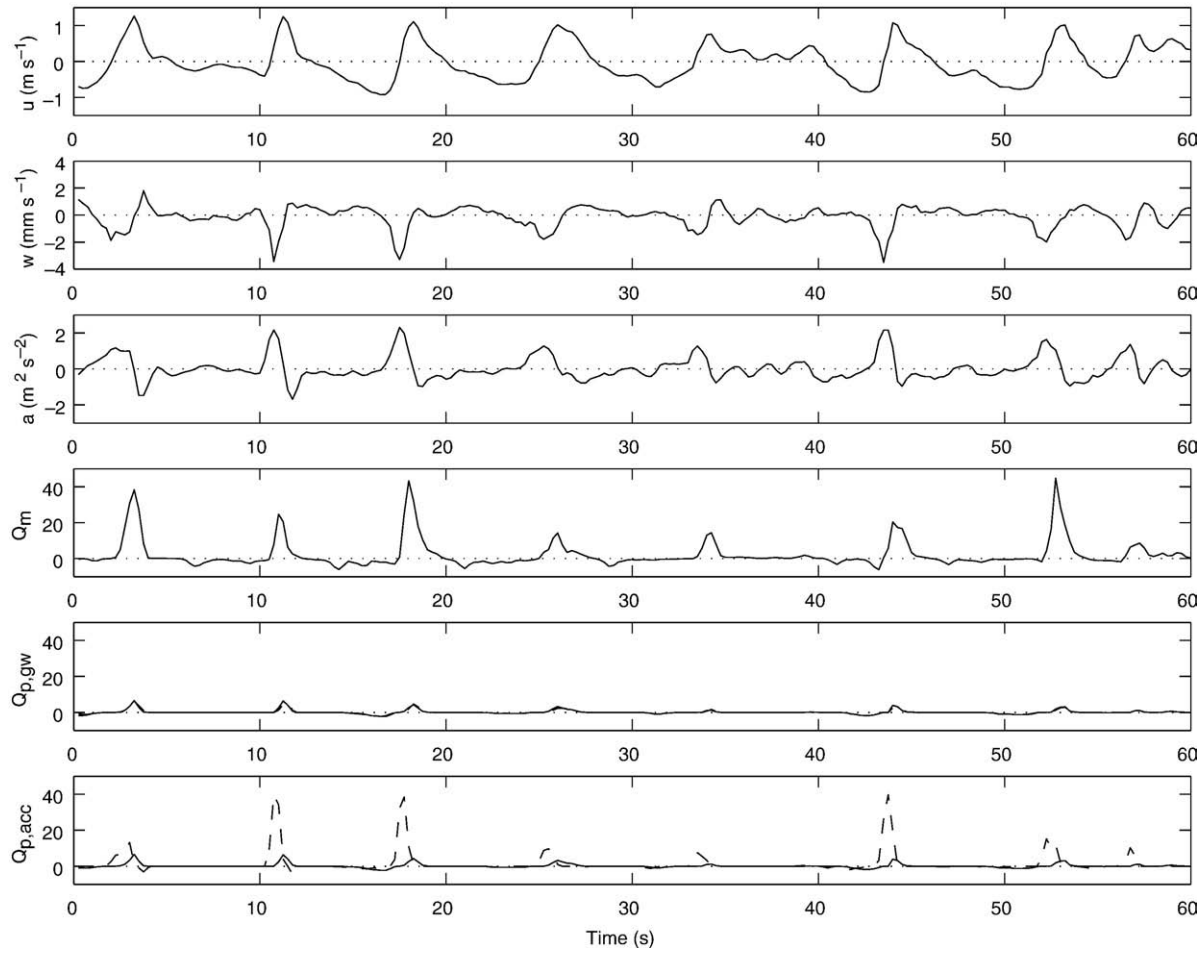

Fig. 10. Example time series collected just before 03:00 h during HT27 showing: cross-shore current velocity u measured at 0.13 m above the bed; vertical flow velocity w; flow acceleration a; measured non-dimensional suspended sediment flux Q_m depth-averaged over the lower 0.15 m of the water column; modelled non-dimensional suspended sediment flux Q_p over the lower 0.15 m of the water column (solid line using standard Shields approach; dashed line accounting for through-bed flow); and modelled non-dimensional suspended sediment flux Q_p over the lower 0.15 m of the water column (solid line using standard Shields approach; dashed line accounting for acceleration using ($\varphi = 50°$).

probably due to the near-bed wave stresses leading the free-stream velocity (cf. Nielsen, 1992). Over a tidal cycle, the inclusion of fluid accelerations correctly predicts the observed net onshore transport and the magnitude of the transport is tuned by optimising the phase angle φ_τ.

The present investigation shows that with the inclusion of fluid accelerations a simple Meyer-Peter-type model can predict onshore transport over prolonged periods of moderate wave conditions reasonably well. Two beaches with very different nearshore hydrodynamic regimes were investigated. At Sennen, the two-dimensional nature of the beachface results in a significant bed return flow. When a standard Shields parameter is input to the Meyer-Peter formula, it results in considerable beachface erosion when measurements show that accretion actually occurred. When acceleration is included, net transport is onshore and qualitatively correct, and quantitatively accurate to within a factor 3. The three-dimensional nature of Truc Vert means that without acceleration, the standard Meyer-Peter approach correctly predicts the direction of the net sediment transport (due to the onshore-directed mean flow over the bar) and in fact provides an almost identical result to the Bailard (1981) model as used by Masselink et al. (2008a); it does however, under predict the transport by a factor 5. Inclusion of acceleration retains the correct directional prediction, but provides a significant quantitative improvement predicting the volumetric change to within a factor 1.2.

Beach morphological change is accomplished by total load transport, so it is interesting to note that the present results provide a reasonable estimate of the morphological change given that the model, originally designed for bed load and sheet flow, was calibrated using only the measured suspended flux. Referring to Section 2.4, at Truc Vert and Sennen, where the Shields parameter during wave events was typically 0.2–0.7 (Masselink et al., 2007b, 2008a), it appears that our measurements were made around the transition to fully developed suspended load conditions and suggesting that transport was a combination of bedload and suspended load. Masselink et al. (2008a) show that the bed load transport rate associated with migrating wave ripples at Truc Vert is of the same order of magnitude as the suspended flux, while at Sennen, Masselink et al. (2007b) obtain a similar result during calm conditions under shoaling waves (although bed load was an order of magnitude less in the surf zone). Therefore, by assuming around 50% of the total load is due to bed load, the measured and modelled fluxes converge.

It is also worth noting that the contribution of the swash zone, where it is well established that suspended sediment concentrations (and thus sediment transport) are more than an order of magnitude higher than the surf zone (Beach and Sternberg, 1991; Miles et al., 2006), and gradients in longshore transport, have been ignored and may also help to explain the difference in measured and predicted flux.

The value of the phase angle φ_τ used during the implementation of the model is important in generating the correct morphological response. Nielsen (1992), on the basis of the monochromatic wave experiments of King (1991), initially suggested an optimum value of

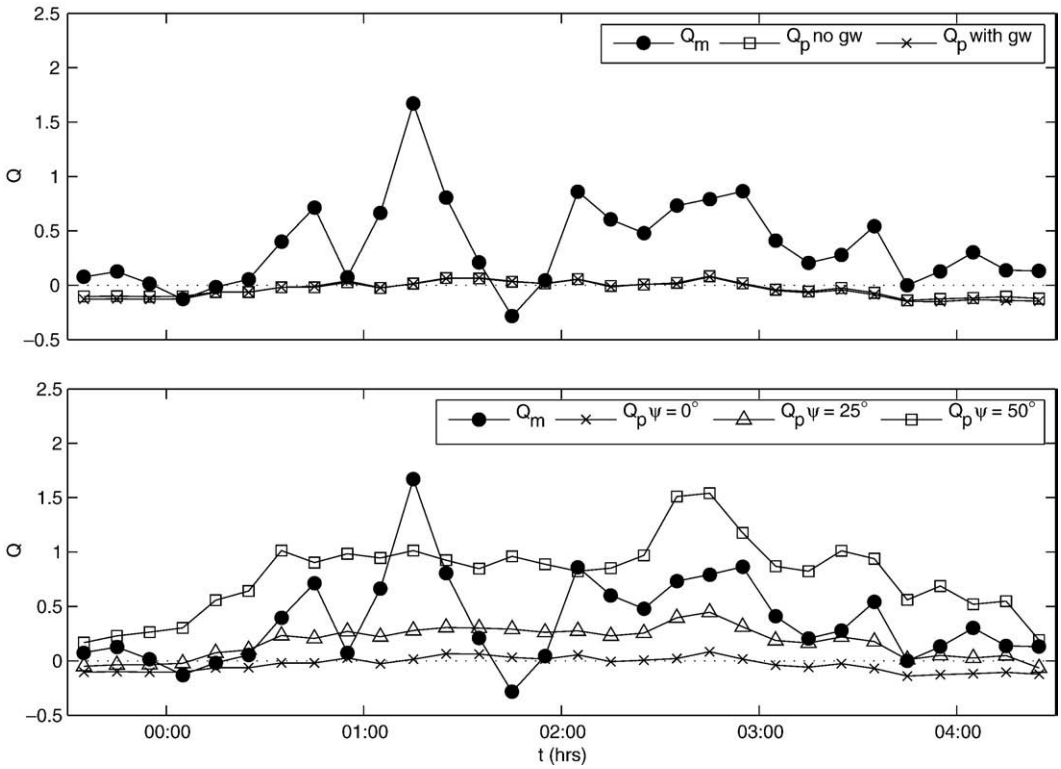

Fig. 11. Comparison of measured and modelled sediment fluxes averaged over 10-min data segments collected during the night high tide of 18–19 May (HT27). Upper panel shows comparison between measured non-dimensional suspended sediment flux Q_m and that predicted using a conventional Shields parameter ($Q_{p,nogw}$) and a Shields parameter modified for bed-through flow ($Q_{p,withgw}$). Lower panel shows comparison between measured non-dimensional suspended sediment flux Q_m and that predicted using a Shields parameter including acceleration (Q_p with $\varphi_\tau = 0$, 25 and 50°).

$\varphi_\tau = 45°$. Subsequently, further optimization using the wave flume data of Watanabe and Sato (2004) (cf. Nielsen, 2006) suggested $\varphi_\tau = 51°$. Our findings suggest that the value of φ_τ optimised for u in the field is 28–35°, appreciably lower than the previous lab-based work; moreover, there is little significant difference between the value of φ_τ used at the different field sites.

It is worth noting that Nielsen and Callaghan (2003) do not recommend the use of the present model over rippled beds where time lags related to vertical sediment movement may become important. However, in the present case, Fig. 6 indicates that the vertical suspended sediment profiles are exponential and indicative of a diffusion-type sediment transport process (Nielsen, 1986). The key point is that the medium and coarse sand sediments ($D_{50} = 0.40$–0.7 mm) settle out before the commencement of the offshore stroke of the wave (cf. Austin and Masselink, 2008, Fig. 7). It could also be argued that the sediments are not actually settling out, but that vortices are being ejected from ripple crests and advected onshore; however, over the almost symmetrical ripples observed here, why is there not offshore advection of vortices during the offshore stroke of the wave thereby countering the onshore flux with an equivalent offshore flux? There are several instances in Fig. 4 where the offshore fluid velocity is of equal or greater magnitude than the onshore flow, yet the suspended sediment concentration is significantly higher during the onshore phase. Therefore the effects encapsulated by the skewed fluid accelerations would appear to be responsible for the onshore transport asymmetry, including any advected vortices.

Bore turbulence has previously been suggested as a mechanism able to cause onshore sediment transport, particularly in the swash and inner-surf zones, and fluid accelerations could potentially act as a surrogate for this turbulence (Puleo et al., 2003; Hsu and Raubenheimer, 2006). It is likely that in the relatively shallow surf zone, bore turbulence would be characterised by the presence of bubbles advected deep into the water column via energetic wave breaking; therefore, turbulence penetrating to the bed would result in the obscuration of the SRP acoustic returns by bubbles. However, if the SRP returns clear acoustic images, bore turbulence is maintained at an elevation at least equal to the mounting elevation of the SRP above the bed (in this case 0.7 m). For the present data, bubble contamination existed for $h < 0.9$ m (cf. Masselink et al., 2007b), probably due to bore turbulence in the inner surf zone; at greater depths the data were uncontaminated suggesting that bore turbulence was not reaching the bed. Moreover, if bore turbulence was the process responsible for the onshore sediment flux, a systematic variation in φ_τ would be expected over each tide due to the presence of bore turbulence in the shallow water at the start and end of each tidal cycle, but not in the deep water over high tide. In fact, no tidal variation in φ_τ occurred at either Sennen or Truc Vert and during the onshore transport events, peak sediment fluxes occurred in the deep water over high tide.

Table 1
Summary of hydrodynamic conditions experienced at Sennen during the tides used for the optimisation of φ_τ

Tide	H_s (m)	T_s (s)	$\langle U_m \rangle$ (m s^{-1})	$\langle a_{spike} \rangle$ (–)	φ_τ (°)
HT06	0.83	7.4	1.34	1.00	42
HT21	0.37	7.5	0.88	2.15	33
HT23	0.32	6.6	0.87	0.912	27
HT27	0.48	7.5	1.21	1.357	36
					Overall: 34.5

6. Conclusions

Field observations of the cross-shore suspended sediment flux have been used to investigate the propensity for wave-driven

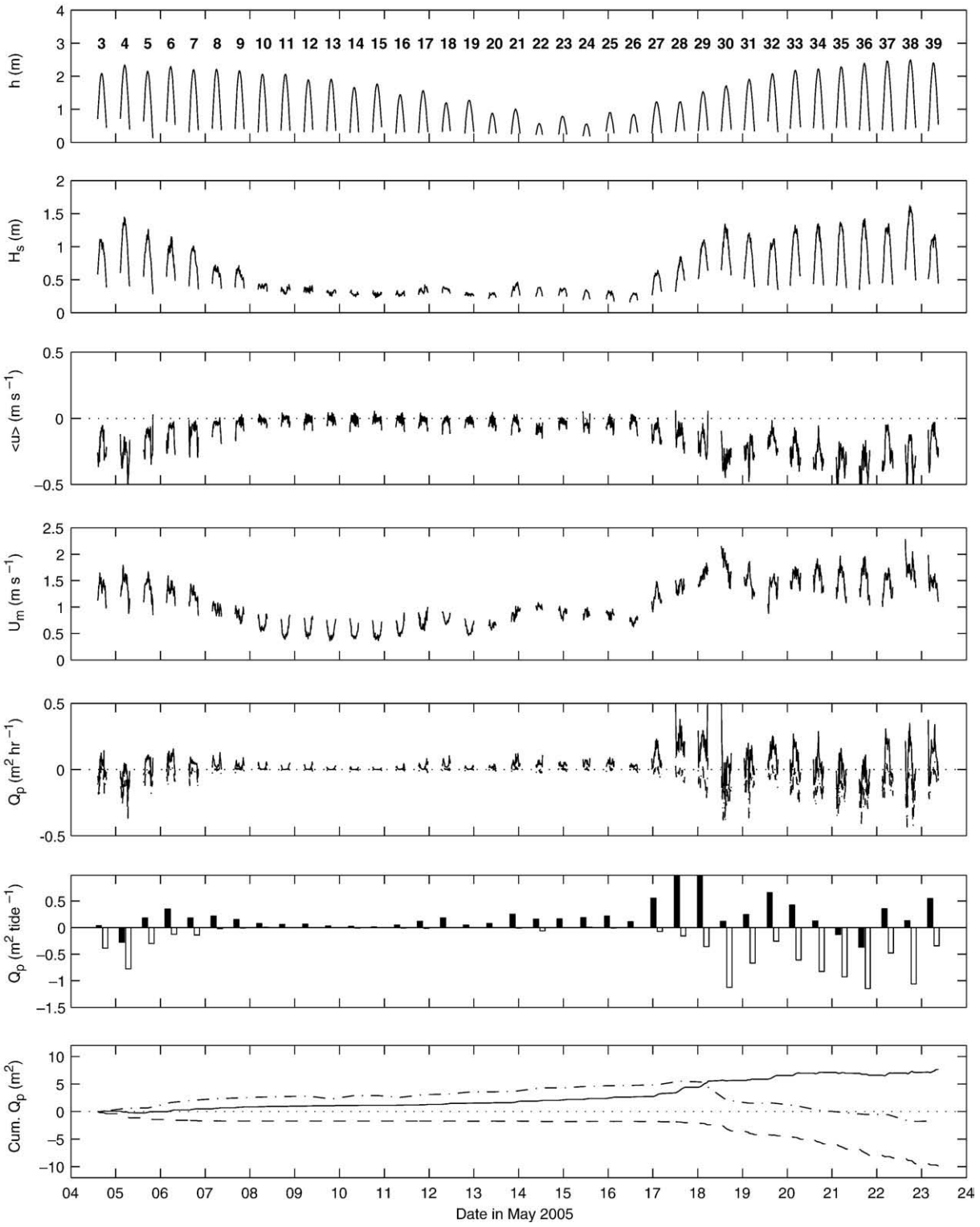

Fig. 12. Predicted cross-shore suspended sediment flux at Sennen accounting for acceleration ($\varphi_\tau = 34.5°$) and ignoring acceleration ($\varphi_\tau = 0°$). From top: water depth h; significant wave height H_s; mean cross-shore flow velocity $\langle u \rangle$; maximum wave orbital velocity U_m; predicted cross-shore suspended sediment flux Q_p; cross-shore transport per tidal cycle; and cumulative flux. The numbers in the upper panel indicate the high tide numbers. Sediment flux with acceleration is indicated by solid line, excluding acceleration dashed line and morphological change by dot-dash line.

onshore-directed sediment transport on beaches during varied energy conditions ($H_s = 0.2$–1.6 m). Three mechanisms capable of causing onshore transport, flow velocity skewness, bed-ventilation and flow acceleration (wave asymmetry) were investigated to determine their relative importance. Flow velocity skewness was discounted since onshore transport was not associated with larger onshore than offshore velocities, whilst the occurrence of peak bed-ventilation at flow reversal resulted in insignificant modifications to the bed shear stress. The onshore-directed flow accelerations under the steep front faces of the asymmetric waves were significantly correlated with the entrainment of sediment from the seabed and therefore onshore sediment transport.

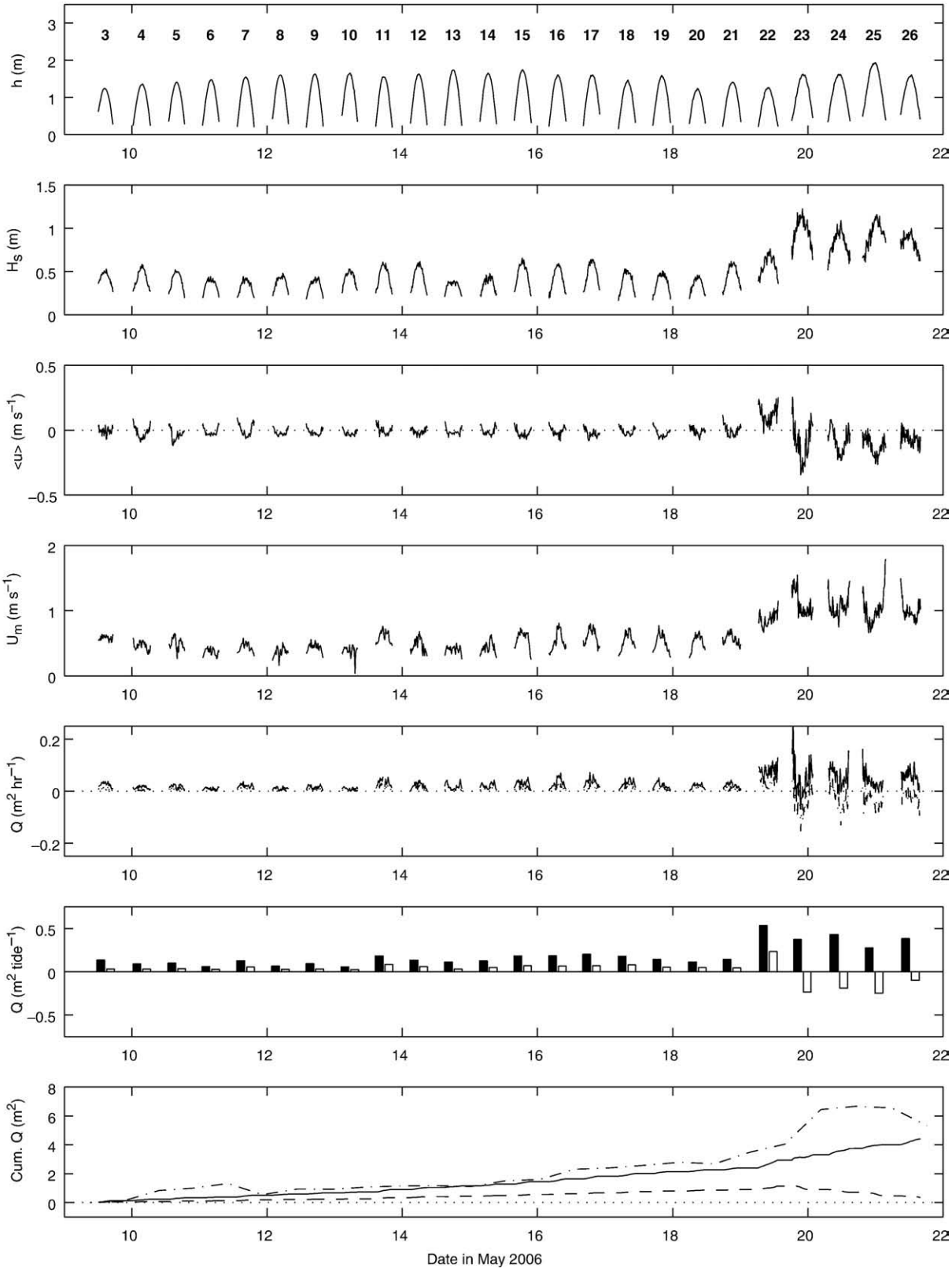

Fig. 13. Predicted cross-shore suspended sediment flux at Truc Vert accounting for acceleration ($\varphi_\tau = 34.5°$) and ignoring acceleration ($\varphi_\tau = 0°$). From top: water depth h; significant wave height H_s; mean cross-shore flow velocity $\langle u \rangle$; maximum wave orbital velocity U_m; predicted cross-shore suspended sediment flux Q_p; cross-shore transport per tidal cycle; and cumulative flux. The numbers in the upper panel indicate the high tide numbers. Predicted sediment flux with acceleration is indicated by solid line, excluding acceleration dashed line and morphological change by dot-dash line.

As an initial attempt to predict the sediment transport a simple sediment transport model that explicitly accounts for fluid accelerations has been used to predict wave-driven cross-shore sediment transport. The Shields parameter was modified to shift the bed shear stress forwards in the wave cycle, thereby accounting for the accelerations around flow reversal. When input to a Meyer-Peter-

type transport formula and calibrated using the field data, the acceleration model provides reasonable qualitative agreement with measured morphological change and predicts the quantitative change to a factor of 1.2 and 3 for a barred and planar beachface, respectively.

Acknowledgements

We would like to thank Peter Ganderton, Tony Butt, Jon Tinker, Tim Scott, Tim Poate, Emma Rendell and Nigel Auger for their expert assistance in the field. Further logistical support was provided at Truc Vert by Nadia Sénéchal and her team from the University of Bordeaux and at Sennen by Nicholas King and the King family. This research was sponsored by the Natural Environment Research Council through grant NER/A/A/2003/00553 'Cross-shore sediment transport and profile evolution on natural beaches (X-Shore)' awarded to PR, GM and TOH. We would also like to thank Daniel Conley for some insightful discussion and Daniel Hanes and an anonymous reviewer for their constructive comments.

References

Aagaard, T., Black, K.P., Greenwood, B., 2002. Cross-shore suspended sediment transport in the surf zone: a field-based parametrization. Mar. Geol. 185, 283–302.
Aagaard, T., Hughes, M.G., Möller-Sorensen, R., Andersen, S., 2006. Hydrodynamics and sediment fluxes across an onshore migrating intertidal bar. J. Coast. Res. 22, 247–259.
Aagaard, T., Nielsen, J., Greenwood, B., 1998. Suspended sediment transport and nearshore bar formation on a shallow intermediate-state beach. Mar. Geol. 148, 203–225.
Ardhuin, F., Herbers, T.H.C., Watts, K.P., van Vledder, G.P., Jensen, R., Graber, H., 2007. Swell and slanting fetch effects on wind wave growth. J. Phys. Oceanogr. 37 (4), 908–931.
Austin, M.J., Masselink, G., 2008. The effect of bedform dynamics on computing suspended sediment fluxes using optical backscatter sensors and current meters. Coast. Eng. 55 (3), 251–260.
Bagnold, R.A., 1966. An approach to the sediment transport problem from general physics. Geological Survey Professional Paper 422-I.
Bailard, J.A., 1981. An energetics total load sediment transport model for a plane sloping beach. J. Geophys. Res. 86, 10938–10954.
Beach, R.A., Sternberg, R.W., 1991. Infragravity driven suspended sediment transport in the swash zone. Proceedings Coastal Sediments '91. ASCE, pp. 114–128.
Bowen, A., 1980. Simple models of nearshore sedimentation; beach profiles and longshore bars. In: McCann, S.B. (Ed.), The Coastline of Canada. Geological Survey of Canada, vol. 80–10, pp. 1–11.
Butt, T., Russell, P.E., Turner, I.L., 2001. The influence of swash infiltration–exfiltration on beach face sediment transport: onshore or offshore? Coast. Eng. 42, 35–52.
Butt, T., Miles, J.R., Ganderton, P., Russell, P.E., 2002. A simple method for calibrating optical backscatter sensors in high concentrations of non-cohesive sediments. Mar. Geol. 192, 419–424.
Butt, T., Russell, P.E., Puleo, J.A., Miles, J.R., Masselink, G., 2004. The influence of bore turbulence on sediment transport in the swash and inner surf zones. Cont. Shelf Res. 24, 757–771.
Conley, D.C., Beach, R.A., 2003. Cross-shore sediment transport partitioning in the nearshore during a storm event. J. Geophys. Res. 108 (C3). doi:10.1029/2001JC001230.
Conley, D.C., Inman, D.L., 1994. Ventilated oscillatory boundary layers. J. Fluid Mech. 273, 261–284.
Davidson, M.A., Huntley, D.A., Holman, R.A., George, K., 1998. The evaluation of large scale (km) intertidal beach morphology on a macrotidal beach using video images. Proceedings International Conference on Coastal Dynamics. ASCE, Copenhagen, pp. 385–394. Denmark.
De Melo Apoluceno, H.H., Dupuis, H., Oggian, G., 2002. Morphodynamics of ridge and runnel systems during summer. J. Coast. Res. SI36, 222–230.
Doering, J.C., Bowen, A.J., 1987. Skewness in the nearshore zone: a comparison of estimates from Marsh McBirney current meters and collocated pressure sensors. J. Geophys. Res. 92 (C12), 13173–13183.
Elgar, S., Guza, R.T., Freilich, M., 1988. Eulerian measurements of horizontal accelerations in shoaling gravity waves. J. Geophys. Res. 93, 9261–9269.
Elgar, S., Gallagher, E.L., Guza, R.T., 2001. Nearshore sandbar migration. J. Geophys. Res. 106 (C6), 11623–11627.
Gallagher, E.L., Elgar, S., Guza, R.T., 1998. Observations of sand bar evolution on a natural beach. J. Geophys. Res. 103, 3203–3215.
Gonzalez-Rodriguez, D., Madsen, O.S., 2007. Seabed shear stress and bed-load transport due to asymmetric and skewed waves. Coast. Eng. 54 (12), 865–930.
Hanes, D.M., Huntley, D.A., 1986. Continuous measurements of suspended sand concentration in a wave dominated nearshore environment. Cont. Shelf Res. 6 (4), 585–596.
Hoefel, F., Elgar, S., 2003. Wave-induced sediment transport and sandbar migration. Science 299, 1885–1887.
Hsu, T., Elgar, S., Guza, R.T., 2006. Wave-induced sediment transport and onshore sandbar migration. Coast. Eng. 53, 817–824.
Hsu, T., Raubenheimer, B., 2006. A numerical and field study on inner-surf and swash sediment transport. Cont. Shelf Res. 26, 589–598.
Huntley, D.A., Hanes, D.M., 1987. Direct measurement of suspended sediment transport. Coastal Sediments '87. ASCE, New Orleans, USA, pp. 723–737.
Karambas, T.V., 2003. Modelling of infiltration–exfiltration effects of cross shore sediment transport in the swash zone. Coast. Eng. J. Jpn. 45, 63–82.
King, D.B., 1991. Studies in oscillatory bed-load sediment transport. Ph.D. thesis, University of California, San Diego (Scripps).
Krumbein, W.C., Monk, G.D., 1942. Permeability as a function of the size parameters of unconsolidated sand. Tech. Rep. 1492, Am. Inst. of Min. and Metal Eng. 11 pp.
Longuet-Higgins, M.S., Parkin, D.W., 1962. Sea waves and beach cusps. Geogr. J. 128, 194–201.
Ludwig, K.A., Hanes, D.M., 1990. A laboratory evaluation of optical backscatterance suspended solids sensors exposed to sand-mud mixtures. Mar. Geol. 94, 173–179.
Marino-Tapia, I.J., Russell, P.E., O'Hare, T., Davidson, M.A., Huntley, D.A., 2007. Cross-shore sediment transport on natural beaches and its relation to sandbar migration patterns: 1. field observations and derivation of a transport parameterization. J. Geophys. Res. 112 (C03001). doi:10.1029/2005JC002893.
Martin, C.S., Aral, M.M., 1971. Seepage force on interfacial bed particles. J. Hydraul. Div., ASCE 7, 1081–1100.
Masselink, G., Short, A.D., 1993. The effect of tide range on beach morphodynamics and morphology: a conceptual beach model. J. Coast. Res. 9 (3), 785–800.
Masselink, G., Auger, N., Russell, P.E., O'Hare, T., 2007a. Short-term morphological change and sediment dynamics in the intertidal zone of a macrotidal beach. Sedimentology 54, 39–53.
Masselink, G., Austin, M.J., O'Hare, T., Russell, P.E., 2007b. Geometry and dynamics of wave ripples in the nearshore zone of a coarse sandy beach. J. Geophys. Res. 112 (C10022). doi:10.1029/2006JC003839.
Masselink, G., Austin, M.J., Tinker, J., O'Hare, T., Russell, P.E., 2008a. Cross-shore sediment transport and morphological response on a macrotidal beach with intertidal bar morphology, Truc Vert, France. Mar. Geol. 251, 141–155.
Masselink, G., Buscombe, D., Austin, M.J., O'Hare, T., Russell, P.E., 2008b. Sediment trend models fail to reproduce small-scale sediment transport patterns on an intertidal beach. Sedimentology. doi:10.1111/j.1365-3091.2007.00917.x.
Meyer-Peter, E., Müller, R., 1948. Formulas for bed-load transport. Report on the 2nd Meeting of the International Association for Hydraulic Structures Research. International Association for Hydraulic Structures Research, Stokholm, Sweden, vol. 2, pp. 39–64.
Miles, J.R., Butt, T., Russell, P.E., 2006. Swash zone sediment dynamics: a comparison of a dissipative and an intermediate beach. Mar. Geol. 231, 181–200.
Nielsen, P., 1986. Suspended sediment concentrations under waves. Coast. Eng. 10, 23–31.
Nielsen, P., 1992. Coastal bottom boundary layers and sediment transport. World Scientific.
Nielsen, P., 1998. Coastal groundwater dynamics. Proceedings Coastal Dynamics '97. ASCE, Plymouth, UK, pp. 546–555.
Nielsen, P., 2006. Sheet flow sediment transport under waves with acceleration skewness and boundary layer streaming. Coast. Eng. 53, 749–758.
Nielsen, P., Callaghan, D.P., 2003. Shear stress and sediment transport calculations for sheet flow under waves. Coast. Eng. 47, 347–354.
Osborne, P.D., Greenwood, B., 1992. Frequency dependent cross-shore suspended sediment transport 1. A non-barred shoreface. Mar. Geol. 106, 1–24.
Puleo, J.A., Holland, K.T., Plant, N.G., Slinn, D.N., Hanes, D.M., 2003. Fluid acceleration effects on suspended sediment transport in the swash zone. J. Geophys. Res. 108 (C11). doi:10.1029/2003JC001943.
Roelvink, J.A., Stive, M.J.F., 1989. Bar-generating cross-shore flow mechanisms on a beach. J. Geophys. Res. 94, 4785–4800.
Russell, P.E., Huntley, D.A., 1999. A cross-shore transport "shape function" for high energy beaches. J. Coast. Res. 15 (1), 198–205.
Schoonees, J.S., Theron, A.K., 1995. Evaluation of 10 cross-shore sediment transport/morphological models. Coast. Eng. 25 (1–2), 1–41.
Sénéchal, N., Bonneton, P., Dupuis, H., 2002. Field experiment on secondary wave generation on a barred beach and the consequent evolution of energy dissipation on the beachface. Coast. Eng. 46, 233–247.
Swart, D.H., 1974. Offshore Sediment Transport and Equilibrium Beach Profiles. Laboratory publication, vol. 131. Delft Hydraulics, Delft. Netherlands.
Thornton, E.B., Humiston, R.T., Birkermeir, W.A., 1996. Bar/trough generation on a natural beach. J. Geophys. Res. 101, 12097–12110.
Turner, I.L., Masselink, G., 1998. Swash infiltration–exfiltration and sediment transport. J. Geophys. Res. 103 (C13), 30,813–30,824.
Watanabe, A., Sato, S., 2004. A sheet flow transport rate formula asymmetric forward leaning waves and currents. Proceedings 29th ICCE. ASCE, Lisbon, pp. 1703–1714.
Wilson, K.C., 1988. Frictional Behaviour of Sheet Flow. Progress Report, vol. 67. Technical University of Denmark, pp. 11–21.